Serine protease NAL1 exerts pleiotropic functions through degradation of TOPLESS-related corepressor in rice

Wenjing Li
Huazhong Agricultural University
Junjie Yan
Huazhong Agricultural University
Yu Zhang
Huazhong Agricultural University
Fei Zhang
Huazhong Agricultural University
Zeyuan Guan
Huazhong Agriculture University https://orcid.org/0000-0002-8909-866X
Yilong Yao
Huazhong Agricultural University
Yu Chang
Huazhong Agricultural University
Haifu Tu
Huazhong Agricultural University
Xiaokai Li
Huazhong Agricultural University
Huaijun Wang
Huazhong Agricultural University
Haiyan Xiong
Huazhong Agricultural University
Xuelei Lai
Huazhong Agricultural University
Ping Yin
National Key Laboratory of Crop Genetic Improvement and National Centre of Plant Gene Research, Huazhong Agricultural University, Wuhan 430070, China https://orcid.org/0000-0001-8001-221X
Lizhong Xiong (lizhongx@mail.hzau.edu.cn)
Huazhong Agricultural University https://orcid.org/0000-0003-0490-1474

Article

Keywords:

Posted Date: August 1st, 2022

DOI: https://doi.org/10.21203/rs.3.rs-1892822/v1

Version of Record: A version of this preprint was published at Nature Plants on June 22nd, 2023. See the published version at https://doi.org/10.1038/s41477-023-01449-2.

Abstract

NAL1 (*NARROW LEAF 1*) is a breeding-valuable pleiotropic gene that affects multiple agronomic traits in rice, but the molecular mechanism is largely unclear. Here, we report that NAL1 is a serine protease and displays a novel hexameric structure whose formation is mediated by ATP-containing positively charged pocket at the N-terminal region. Moreover, we identified TOPLESS-related corepressor OsTPR2 involved in multiple growth and development processes as the substrate of NAL1. We found that NAL1 degraded OsTPR2, thus modulating the expression of downstream genes related to hormone signaling pathways, eventually achieving its pleiotropic physiological function. An elite allele $NAL1^{A}$ originated from wild rice could increase grain yield. Furthermore, the *NAL1* homologs in different crops have a similar pleiotropic function to *NAL1*. Our study uncovers a NAL1-OsTPR2 regulatory module and provides gene resources for the design of high-yield crops.

Introduction

Rice is a staple food for more than half of the world's population, but global food security still faces great challenges in the future due to the continuous increase in population and decrease in arable land[1]. Crop yield is a genetically complex trait consisting of numerous traits, and pleiotropy is defined as one gene influencing multiple traits. For example, *IPA1* (I*deal* P*lant* A*rchitecture 1*), encoding a SPL (SQUAMOSA promoter-binding protein-like) transcription factor, regulates different downstream genes, thereby enhancing effective tiller, panicle branching, and disease resistance, ultimately improving rice yield[2]. *Ghd7* (G*rain number, plant* h*eight and heading* d*ate 7*), encoding a CCT-domain transcription factor, increases grain number, plant height and nitrogen use efficiency by repressing the expression of *OsTB1, ARE1*, and other genes involved in the floral transition and lateral branch development[3–5]. These pleiotropic genes have been widely used in modern rice breeding[6]. Therefore, the employment of pleiotropic genes simultaneously enhancing multiple agronomic traits is an effective approach in crop breeding.

NAL1 is a pleiotropic gene identified by multiple genetic analyses in rice. Significant loci containing *NAL1* have been identified by analyzing different traits (grain yield, plant architecture, leaf morphology, root architecture, photosynthesis rate, chlorophyll content) via genome-wide association study (GWAS) in different natural populations[7–11]. A major quantitative trait loci (QTL) allelic to *NAL1* has been detected in different recombinant inbred lines or near-isogenic lines related to flag leaf traits, grain yield, chlorophyll content, and source leaf/sink capacity traits[12–17]. A major natural variation associated with the pleiotropic function has been identified to be an A-to-G substitution in the coding region of *NAL1*, resulting in the conversion of amino acid His233 into Arg233 (H233R), and the biological function of *NAL1* in controlling the pleiotropic traits has been confirmed using transgenic or introgression lines[7,15,18]. *NAL1* is expressed in all organs such as roots, leaf sheaths, leaves, culms, and young panicles. NAL1 protein contains a nuclear localization signal in its C-terminus, and it has been found to be concentrated in nuclear protein bodies[19]. The studies of different *nal1* mutants have revealed that *NAL1* affects cell

division and expansion, thus influencing leaf width and adventitious root development. Furthermore, in *nal1* mutants, the expression levels of genes involved in auxin transport and signaling are changed greatly[19–22]. Recently, FZP (FRIZZY PANICLE) has been reported as a target of NAL1 to regulate secondary branching of inflorescences and grain yield in rice[23]. In barley, a putative cyclophilin-type HvPPIase has been identified to interact with HvNAL1 to regulate tiller number and leaf morphology[24]. Nevertheless, the molecular mechanism by which *NAL1* regulates the multiple traits remains largely unknown.

The TPL/TPR (TOPLESS/TOPLESS-related) family proteins, belonging to Groucho/Tup1-type corepressors, are involved in hormone signaling pathways and other transcriptional regulation processes, thus affecting multiple traits such as plant height, leaf architecture, tiller number, and spike development[25]. Different transcriptional repressors/adaptor proteins and histone deacetylase (HDACs) bind TPL/TPR family proteins respectively through LisH domain in the N terminus and the WD40-repeat domain in the C terminus to form complexes, and these resulting complexes decrease histone acetylation levels of downstream genes and repress their expression[26–29]. TPL/TPR family proteins are pivotal for plant development, and thus the fine-tuned regulation of protein activity and stability is important for the exertion of their suppressive function[30]. A recent report on *Arabidopsis* has shown that SUMOylation of TPR1 represses its activity and inhibits the constitutive activation of immune responses under non-pathogenic conditions[31]. However, how TPL/TPR protein levels are regulated to relieve the repression of downstream gene expression remains unclear.

In this study, we biochemically reconstituted NAL1 *in vitro* and solved its crystal structure. We found that NAL1 displayed a hexameric structure, and that ATP molecule played a key role in its oligomeric assembly. Structure comparison and biochemical assays suggested that NAL1 was a new plant-specific serine protease. We also found that NAL1 interacted with OsTPR2 (a TPL/TPR member in rice) via its C-terminal EAR-like motif to promote OsTPR2 degradation. OsTPR2 degradation by NAL1 increased the histone acetylation levels of the genes in auxin and strigolactone (SL) signaling pathways as well as development-related genes, thus up-regulating the expression of these genes. In addition, we found that an elite allele $NAL1^{A}$ with a variation at the catalytic triad of the protease, originated from common wild rice (*Oryza. rufipogon*), was selected during rice breeding.

Results

Crystal structure determination of NAL1 hexamer

In the past decade, several studies have demonstrated the pleiotropic roles of *NAL1* in agronomic traits, and it has been identified as a valuable gene in rice breeding[9,12,15]. In order to unveil NAL1 pleiotropic mechanism, we performed protein structure analysis since sequence alignment of NAL1 against known proteins could not predict a reliable biochemical function. The crystal structure of NAL1 (residues 59-463) was determined at a resolution of 2.6 Å (Fig. 1a, Extended Data Fig. 1a and Extended Data Table 1).

Electron density of residues 78-84, 175-183, and 407-412 was undetectable, which might be due to their flexibility in solution. NAL1 was trimeric in one unit cell (Extended Data Fig. 1b), and NAL1 hexamer was assembled from two symmetric neighboring unit cells (Fig. 1a). The protomers of NAL1 shared almost identical architectures without apparent structural variation (Extended Data Fig. 1c). To further validate the oligomeric state of NAL1, analytical ultracentrifugation (AUC) experiments were performed. The results showed that the full-length NAL1 was mainly in a hexameric state, which was consistent with the crystallographic analysis (Extended Data Fig. 1d).

Dali (a structure comparison server) search revealed that NAL1 was a serine protease according to the structural similarity (Extended Data Fig. 1f, and Extended Data Table 2). Thus, each NAL1 protomer was divided into two segments: N-terminal domain (NTD, residues 59-197) and C-terminal serine protease domain, consisting of 10 α-helices and 22 β-sheets (Extended Data Fig. 1a, e). Within the NTD, an ATP molecule was found in a pocket surrounded by a3, a4, b4, and a loop (Fig. 1b, Extended Data Fig. 2a), and this pocket was stabilized by a positively charged network consisting of residues R120, R122, K123, K139, and K142 (Fig. 1c). This ATP molecule expelled a3 from one protomer to another, thus leading to a cation-p interaction between W144 and H248 from the neighboring protomers, eventually mediating the formation of a trimer. Our results showed that the oligomerization was abolished by W144A point mutation, further validating role of the cation-p interaction in oligomerization (Extended Data Fig. 2b). Further, we investigated the effect of the residues surrounding ATP on NAL1 oligomerization. The mutation of either R120 or R139 into alanine disrupted the oligomerization (Extended Data Fig. 2b), suggesting that ATP could mediate the oligomerization of NAL1.

The C-terminal serine protease domain of NAL1 consisted of two perpendicular six-stranded β-barrel subdomains, and the putative catalytic triad was composed of H233, D291, and S385, which were located in the crevice between the two lobes (Fig. 1d, Extended Data Fig. 2c). We noticed that the natural single nucleotide variation (A-to-G substitution) of *NAL1* occurred exactly in the catalytic triad, resulting in the conversion of His233 to Arg233 (H233R), which was found to be associated with the pleiotropic traits[11,17]. In this study, we designated the two alleles of *NAL1* as $NAL1^{A}$ (H233) and $NAL1^{G}$ (R233), respectively. To genetically examine the functional differences between the alleles, we constructed two complementary lines $NAL1^{A}$-COM and $NAL1^{G}$-COM in the *NAL1*-knockout mutant (*nal1-cri*) background generated by CRISPR-Cas9 technique. Both complementary lines partially recovered phenotypes of *nal1-cri*, but the $NAL1^{A}$-COM line showed significantly stronger phenotypes than the $NAL1^{G}$-COM line, including wider flag leaf, higher plant height, larger root, larger panicle, and higher grain yield (Fig. 1e-j). These results suggested that the $NAL1^{A}$ was a genetically stronger allele, and that the H233 in the catalytic triad might be a critical residue for NAL1 functions.

NAL1 physically interacts with OsTPR2

To unveil the underlying mechanism of *NAL1*'s pleiotropic functions, immunoprecipitation in combination with mass spectrometry (IP-MS) was used to identify NAL1-interacting proteins. Of the detected

31 proteins (Extended Data Table 3), 3 TPR family proteins (OsTPR1/2/3) were selected for further research since they regulate multiple growth and development processes[28,32].

To verify the interaction between NAL1 and OsTPR family proteins, we performed luciferase complementation imaging (LCI) assays in *Nicotiana benthamiana* leaves. The previously reported *NAL1* mutant (*nal1-1*) with 10-AA deletion in the serine protease domain[19] was used as a negative control. We found that NAL1, rather than *nal1-1*, interacted with all the three rice TPR proteins (Extended Data Fig. 3a). *OsTPR2* was selected for further investigation since this gene has been reported to be involved in regulating multiple developmental and agronomic traits[33-36]. Bimolecular fluorescence complementation (BiFC) assays showed that YFP fluorescence signal was detected in the cells co-expressing OsTPR2-nYFP and NAL1-cYFP, but not in the cells co-expressing OsTPR2-nYFP and nal1-1-cYFP (Fig. 2a). In addition, NAL1-GFP was co-immunoprecipitated with OsTPR2-Flag when they co-expressed in tobacco leaves (Fig. 2b). All above results suggested the interaction between NAL1 and OsTPR2.

OsTPR2 was divided into N-terminal TPD domain and C-terminal WD40 domain according to previous reports[32,37]. LCI assay was performed to further determine which domain of OsTPR2 interacted with NAL1. The results showed that TPD, rather than the WD40 domain, interacted with NAL1 (Fig. 2c), implying that N-terminal TPD domain mediated the interaction between NAL1 and OsTPR2. Previous reports show that TPD interacts with proteins via an EAR-motif (LXLXL)[38-41]. We detected two EAR-like motifs (EAR-1: 558-MSLHLGD-564; EAR-2: 576-SSLDLEK-582) in the C-terminus of NAL1 (Fig. 2d, Extended Data Fig. 3b). To further determine whether these two EAR-like motifs mediated the interaction between NAL1 and OsTPR2, a truncated NAL1 with the two EAR-like motifs deleted (residues 1-559) was constructed. Gel filtration assays showed that the deletion of two EAR-like motifs completely abolished the interactions (Extended Data Fig. 3c). Point mutations at the EAR-1 motif disrupted their interaction (Fig. 2d), whereas those at the EAR-2 motif did not (Extended Data Fig. 3c), suggesting the key role of EAR-1 in the interaction between NAL1 and OsTPR2. To further decipher the interaction mechanism between $NAL1^{EAR-1}$ and OsTPR2, we modeled a OsTPR2-$NAL1^{EAR-1}$ complex structure, in which L560 and L562 of $NAL1^{EAR-1}$ exhibited a hydrophobic interaction with F74, F104, L118, L130 of OsTPR2 (Extended Data Fig. 3d, e). Taken together, NAL1 C-terminal EAR-like motif and OsTPR2 N-terminal TPD domain jointly mediated the interaction between NAL1 and OsTPR2.

NAL1 promotes degradation of OsTPR2

To test whether NAL1, a structurally distinct serine protease, is capable of degrading OsTPR2, *in vivo* protein degradation assays were performed using rice protoplasts. The results showed that OsTPR2 was hardly degraded in *nal1-cri* protoplasts, whereas ~50% OsTPR2 was degraded within 5 h in the wild type (ZH11). As a negative control, GFP protein exhibited no change in *nal1-cri* and ZH11 protoplasts (Fig. 2e, Extended Data Fig. 4a). Moreover, the same assays were performed in the *nal1-1* mutant and its

corresponding wild type (rice cultivar ZF802)[19], and similar results were observed (Extended Data Fig. 4b). Overall, our results showed that NAL1 could facilitate the degradation of OsTPR2 *in vivo*.

Subsequently, recombinant 6×His-tagged OsTPR2 was used as substrate to investigate its degradation by NAL1 in cell-free extracts from *nal1-cri* and wild type ZH11 plants. Compared to ZH11, the degradation of OsTPR2 was delayed in the *nal1-cri* extract (Fig.2f, Extended Data Fig. 4c). Similar results were observed in the assays of cell-free extracts of *nal1-1* mutant and wild type ZF802 plants (Extended Data Fig. 4d). These results further suggested that NAL1 could promote OsTPR2 degradation. To further confirm whether NAL1 functions biochemically as a serine protease, different protease inhibitors were added into ZH11 cell-free extracts to examine the degradation of OsTPR2. The results showed that all the 3 serine protease inhibitors phenylmethanesulfonyl fluoride (PMSF), aprotinin, and leupeptin could almost abolish OsTPR2 degradation. In contrast, the metalloprotease inhibitor bestatin, the aspartic protease inhibitor pepstain, or the cysteine protease inhibitor E-64 could not inhibit OsTPR2 degradation (Fig. 2g, h). These results strongly suggested that NAL1 was a *bona fide* serine protease.

To examine the importance of the catalytic triad to the proteolytic activity of NAL1, wild type NAL1 and the triad-mutated NAL1 (mNAL1) were incubated with OsTPR2 *in vitro,* respectively. The results showed that wild type NAL1 degraded ~50% OsTPR2 within 1 h, whereas mNAL1 exhibited highly compromised degradation activity (Fig. 2i, Extended Data Fig. 4e). To further reveal the function of the catalytic triad of NAL1 in plants, we examined the proteolytic activity in the previously reported near isogenic lines NIL-IR and NIL-ZS containing the alleles $NAL1^A$ and $NAL1^G$, respectively[17]. *In vivo* and cell-free protein degradation assays both showed that NAL1 protein from $NAL1^A$ allele had stronger proteolytic activity than that from $NAL1^G$ (Fig. 2j, k). In addition, the OsTPR2 abundance quantified by the anti-OsTPR2 antibody was significantly higher in *nal1-cri* than in ZH11 (Extended Data Fig. 4f), while the *OsTPR2* mRNA level showed no difference between *nal1-cri* and ZH11 (Extended Data Fig. 4g). These results suggested the importance of the catalytic triad to the proteolytic activity of NAL1.

To clarify the genetic interaction between *NAL1* and *OsTPR2*, we constructed OsTPR2 RNA interference (RNAi) lines in the *nal1-cri* background. The expression level of *OsTPR2* in three positive OsTPR2-RNAi/nal1-cri lines was decreased to approximately half of that in *nal1-cri* (Extended Data Fig. 5a). Compared to those in *nal1-cri*, plant height, flag leaf width, root dry weight, and grain yield were significantly increased in the three OsTPR2-RNAi/nal1-cri lines (Fig. 3a-f). These results suggested that the pleiotropic function of *NAL1* genetically depended on *OsTPR2*, which was consistent with the biochemical relationship between NAL1 and OsTPR2.

NAL1 exerts pleiotropic function by alleviating OsTPR2-mediated hormone signaling pathway suppression

TPL/TPR family proteins have been reported to regulate hormone signaling pathways by forming complexes with repressors and transcription factors, thus affecting histone acetylation levels of

downstream target genes in *Arabidopsis*[26-28,32,34,38,39]. To determine whether the rice homologs share the same mechanism, we investigated the potential complex formation from OsIAA3/17 (identified by a yeast-two-hybrid screening of OsTPR2), OsARF25 (OsIAA3/17-interacting transcription factor in auxin signaling pathway)[42,43], and OsTPR2 by *in vitro* pull-down assays. Meanwhile, the repressor D53[34] and its corresponding transcription factor IPA1[44] in SL signaling pathway were selected for examining their interactions with OsTPR2. The results showed that GST-tagged OsARF25 (or IPA1) was co-eluted with 6×His-tagged OsIAA3/17 (or D53) and StrepII-tagged OsTPR2, but not with StrepII-tagged OsTPR2 alone (Fig. 4a-c), suggesting that OsTPR2 might participate in the regulation of hormone signaling by forming a TF-adaptor-TPR complex like their homologs in *Arabidopsis*. Since NAL1 promoted OsTPR2 degradation, we speculated that NAL1 might affect histone acetylation, thus alleviating the OsTPR2-mediated suppression of genes in the hormone signaling pathways. To test the speculation, the histone acetylation levels in ZH11 and *nal1-cri* were examined. H3Ac, H3K9Ac, and H3K18Ac levels were lower in *nal1-cri* than in ZH11, with H3K18Ac exhibiting the most significant difference (Fig. 4d). Furthermore, a total of 13277 genes were found to have a lower H3K18Ac level in *nal1-cri* than in ZH11 by ChIP-seq analysis. Based on the published RNA-seq data of *nal1* mutant and its wild type[20], 902 genes whose expressions were down-regulated in the *nal1* mutant[20] also showed decreased H3K18Ac levels (Extended Data Fig. 5b, and Extended Data Table 4), further supporting that NAL1 fulfilled its pleiotropic functions by alleviating the OsTPR2-mediated gene expression suppression.

To further clarify how the NAL1-OsTPR2 module regulated gene expression, we investigated *OsARF25*-targeted genes (*PIN1b*, *ERF3* and *CKX4*) in auxin signaling pathway and IPA1-targeted genes (*SLR1* and *DEP1*) and *CKX9* (affected by D53, but not the target gene of IPA1) in SL signaling pathway. The genome browser data showed that H3K18Ac level of these genes was significantly lower in *nal1-cri* than in ZH11, which was confirmed by H3K18Ac-ChIP qPCR assays (Fig. 4e, f, Extended Data Fig. 4c, d). We examined the effects of *NAL1* on the expression of these genes. As expected, these genes showed lower expression in *nal1-cri* than in ZH11 (Fig. 4g). In the double mutant OsTPR2-RNAi/nal1-cri lines, down-regulating *OsTPR2* partially alleviated the expression suppression of above-mentioned genes, compared to *nal1-cri* (Fig. 3g). These results jointly implied that NAL1 positively modulated histone acetylation and gene expression by degrading the co-repressor OsTPR2.

NAL1 and its homolog genes in other crops are highly breeding-valuable

In previous studies, the natural variation of *NAL1*, mainly two haplotypes corresponding to the alleles $NAL1^A$ and $NAL1^G$, is genetically detected in cultivated Asia rice varieties[10,11,15]. The difference of their protease activity (Fig. 1, 2) was in accordance with their biological function *in vivo*. It has been reported that the stronger allele $NAL1^A$ is derived from the weaker allele $NAL1^G$ in the ancestral population and has undergone artificial selection[8,18,45], but its detailed origin route is still unknown. Therefore, we analyzed whole-genome sequencing data of a large panel of accessions including 3243 *O. sativa* varieties and 460

O. rufipogon accessions[46,47]. *NAL1*^{A} exists in 71.39% of *japonica* rice varieties, but only in 1.67% of *indica* rice varieties, indicating that the *NAL1*^{A} might be population-specific. *Indica* and *japonica* have been reported to be descended from common wild rice *Or-I* and *Or-III*, respectively[46]. We noticed that *NAL1*^{A} existed only in 2 *Or-III* accessions, but *NAL1*^{G} existed in all the *Or-I* accessions (Fig. 5a, Extended Data Fig. 6a), implying that *NAL1*^{A} in *japonica* rice was originated from *Or-III* wild rice. Single-nucleotide diversity analysis showed that the diversity of *japanica* was almost 20 folds higher that of *Or-III*, but *indica* did not significantly differ from *Or-I* (Extended Data Fig. 6b), indicating that *NAL1*^{A} might undergo artificial selection during *japanica* rice domestication, which is consistent with previous report[45].

Since almost all *indica* rice varieties contain the weak allele *NAL1*^{G}, we wondered whether the functionally strong allele *NAL1*^{A} has potential in *indica* rice breeding. To this end, we introduced the *NAL1*^{A} allele into Huang-hua-zhan (HHZ), an elite *indica* variety widely cultivated in China, to replace its *NAL1*^{G} allele. Morphological traits including plant height, flag leaf width, root and panicle size were significantly improved in the near-isogenic line HHZ-NAL1^{A}, compared to those in HHZ. As a result, grain yield per plant was significantly increased (Fig. 5b-g), indicating promising application value of the *NAL1*^{A} allele in *indica* rice breeding.

Since *NAL1* is a breeding-valuable pleiotropic gene in rice, we further examined the conservativeness of the function of its homologs in other crops. A phylogenic tree of NAL1 and its homolog proteins from wheat, maize, soybean, and rapeseed showed that all the four crops had homologs of *NAL1* (Extended Data Fig. 7a). One homolog from each crop was selected to complement *nal1-cri*. Compared to *nal1-cri*, the complementary lines exhibited significant recovery in plant height, flag leaf morphology, root system, and grain yield (Extended Data Fig. 7b-g), indicating that the *NAL1* homologs from main crops may have conserved functions.

Discussion

Although numerous genetic studies of *NAL1* in rice have been reported, the molecular mechanism by which *NAL1* regulates plant growth and development remains unknown. Here, we revealed the crystal structure and biochemical function of NAL1, providing direct evidence that NAL1 was a *bona fide* serine protease (Fig. 1, 2). The protein domain organization of NAL1 is reminiscent of the well-known high temperature requirement A (HtrA) serine proteases which generally consist of one protease domain and one or two PDZ domains, and the protease domain of HtrA is critical for its cage-like oligomerization (Extended Data Fig. 1g)[48]. Different from HtrA family proteases, NAL1 forms a stacked trimeric ring under mediation of both protease domain and the NTD in which ATP molecule is found to be located in a positively charged pocket (Fig. 1, Extended Data Fig. 2). This special oligomeric architecture suggested that NAL1 was a serine protease with a new hexameric structure. ATP is required for NAL1 oligomeric assembly, suggesting a possible correlation between oligomerization and the plant energetic states, but it still needs further investigation.

Since NAL1 is a serine protease, the identification of its potential substrate is important for understanding its pleiotropic mechanism. However, identification of protease substrates is challenging mainly because of the momentary nature of the interaction and instability of the substrates[49]. Using IP-MS, we identified several NAL1-interacting proteins including OsTPR family members from NAL1-Flag overexpressing lines. In addition, we found that the interaction between NAL1 and OsTPR2 was mediated by both NAL1 C-terminal EAR-like motif and OsTPR2 N-terminal TPD domain (Fig. 2, Extended Data Fig. 3), and this binding mode is consistent with previous reports[40,41,50]. TPL/TPR family proteins play important roles in numerous developmental processes, and they can form transcriptional repression complexes to modulate multiple hormone signaling pathways[25]. Therefore, controlling TPL/TPR protein homeostasis is important for plant growth. The quality control of repressors involved in plant hormone signaling is mostly dependent on ubiquitination degradation system[51]. Our *in vivo* and cell-free protein degradation assays showed that OsTPR2 was proteolytically degraded by NAL1 (Fig. 2, Extended Data Fig. 4), which was distinct from the ubiquitination degradation. This finding extends our knowledge of protein homeostasis regulation of important repressors.

In *Arabidopsis*, the canonical TF-adaptor-TPL/TPR regulatory modules function in auxin, jasmonic acid (JA), SL signaling pathways[25]. The canonical ARF-IAA-TPL/TPR complex in auxin signaling and MYC2-JAZ/NINJA-TPL/TPR complex in JA signaling have been intensively investigated for their roles in regulating plant growth, development, and stress responses[28,39,52,53]. In SL signaling, TPL/TPR has been reported to interact the adaptor protein SMXL and unknown TFs to regulate SL-responsive genes[34,54]. In this study, the canonical regulatory modules OsARF25-IAA3/17-OsTPR2 and IPA1-D53-OsTPR2 in rice were identified (Fig. 4), implying that TF-adaptor-TPL/TPR might be a conserved regulation module in both monocot and dicot plants.

The NAL1-OsTPR2 module regulates the expression of auxin and SL signaling genes such as *PIN1b*, *ERF3*, *CKX4*, *SLR1*, *DEP1*, and *CKX9* (Fig. 4). *PIN1b* is involved in the development of adventitious root, and it is a downstream gene of *OsARF25* and *IPA1*[44,55]. In this study, we found that *PIN1b* histone acetylation was regulated by OsARF25-IAA3/17-OsTPR2 and/or IPA1-D53-OsTPR2 modules (Fig. 4), providing insight into how *PIN1b* is involved in the crosstalk between auxin and SL signaling. *CKX4* and *CKX9* play a pivotal role in crown root formation and shoot architecture[43,56,57]. *ERF3* promotes crown root elongation[42,58]. *SLR1* and *DEP1* have been reported to be involved in rice shoot and panicle development[44]. In addition to the genes involved in hormone signaling, we also examined the expression of *ACL1*, a downstream gene of *URL1-OsTPR2*, involved in leaf development[35]. Our results showed that the expression of *ACL1* was decreased in *nal1-cri*, but this decrease was alleviated in OsTPR2-RNAi/nal1-cri lines (Extended Data Fig. 8), which further supported the phenotypes of OsTPR2-RNAi/nal1-cri lines that were partially recovered compared to *nal1-cri* (Fig. 3). Knockout of OsTPR2 resulted in severe developmental defects and even infertility, which deprived us of exploring their genetic interaction by *OsTPR2* knockout. In addition, other NAL1-interacting proteins or substrates including the paralogs of OsTPR2 (OsTRP1/3) (Extended Data Table 3) might also partially contribute to the pleiotropic

phenotypes. For example, FZP regulating the secondary panicle branches could be degraded by NAL1[23], but this protein was not identified in our IP-MS experiment. Therefore, we cannot rule out the possibility that there might exist other NAL1 substrates, and further investigation of these potential substrates is likely to provide insight into *NAL1*'s pleiotropic function. Taken together, we propose a simplified working model for the NAL1-OsTPR2 module. NAL1, as a plant-specific serine protease, can directly degrade the co-repressor OsTPR2, thereby resulting in the increase of histone acetylation level and expression levels of downstream genes related to hormone signaling pathways (such as auxin and SL examined in this study), ultimately modulating plant growth and development and improving multiple agronomically important traits such as plant, leaf, and root architecture, and grain yield (Fig. 6).

The natural variation (*NAL1*^{A} to *NAL1*^{G}) was found to change one of the catalytic triad (H233 to R233), and our genetic complementation assays indicated the importance of H233 for NAL1 proteolytic activity (Fig. 1). This might be the main reason why *NAL1*^{A}/*NAL1*^{G} alleles were identified by GWAS of different traits[7–11]. In addition, both *in vivo* and *in vitro* protein degradation assays showed that NAL1 protein encoded by *NAL1*^{A} allele had higher proteolytic activity than that encoded by *NAL1*^{G} (Fig. 2, Extended Data Fig. 4). *NAL1*^{A} allele originated from wild rice might undergo artificial selection in *japonica* rice cultivars, but not in *indica*. Interestingly, *NAL1*^{A} exhibited a potential in promoting agriculture traits as evidenced by introgression lines (Fig. 5)[12,15]. In addition, *NAL1*^{A} can also increase nitrogen use efficiency in *indica* rice background[45]. However, a recent study has revealed that the weak allele *NAL1*^{G} is conducive to the maintenance of the balance between leaf photosynthesis and plant architecture for increasing biomass and grain yield under low planting density in *indica* rice variety 9311[59]. Compared to *japonica*, *indica* rice cultivar has been conventionally planted with lower plant density. Therefore, we speculate that *NAL1*^{A} may have been selected during *japonica* rice domestication because of its stronger pleiotropic function leading to a relatively more compact architecture, thus allowing high-density planting. Nevertheless, the detailed origin and selection mechanism of *NAL1*^{A} deserves further studies.

NAL1 is a plant-specific serine protease and its homologs are highly conserved. Our genetic complementation experiments indicated that *NAL1* genes had conservative function in main crops (Extended Data Fig. 7). Recently, *NAL1* homologs in barley and sugarcane have also been reported to affect leaf width[24,60]. However, there are no reports that *NAL1* homologs affect agronomic traits in main crops except rice. Interestingly, protein sequence analysis showed that the amino acid residues corresponding to H233 (or R233) of NAL1 were all arginine in the other main crops (Extended Data Fig. 9). In addition, we found no natural variation altering this amino acid residue based on sequencing databases from other species. It will be interesting to explore why the H233R variation occurs only in rice and whether there are potential important variations at NAL1 other sites in the plants. Our data showed that the grain yield of *NAL1*^{A} complementary line was significantly higher than that of *NAL1*^{G} and *NAL1*-homologs complementary lines (Fig. 1, Extended Data Fig. 7), indicating that the function of *NAL1*^{A} was not only stronger than that of *NAL1*^{G} but also than that of the *NAL1* homologs from other main crops. Thus, we propose that the functionally stronger allele of *NAL1* may be used to improve agronomic traits

of other crops by gene editing technology. In summary, this study reveals the molecular mechanisms by which NAL1-OsTPR2 module regulates rice growth and development and identifies the key residues affecting NAL1 proteolytic activity, and these findings are valuable for crop breeding design.

Methods

Materials

To construct *NAL1*-knockout line by CRISPR/Cas9 technology, the 20 bp specific sgRNA target sequence of *NAL1* was designed and cloned into the *TKC* vector driven by OsU6 promoter [61], and then the resultant vector was transformed into rice calli of wild type Zhonghua11 (ZH11, *O. sativa* ssp *japonica*) through Agrobacteria-mediated transformation. The homozygous mutants, named *nal1-cri*, were identified by sequencing and PCR. Primers used were shown in Extended Data Table 5.

To construct the complement lines in *nal1-cri* background, NAL1 homologs from maize, wheat, soybean and rapeseed, $NAL1^A$, and $NAL1^G$ were cloned into *pCAMBIA2300* vector and these genes were driven by *NAL*1 native promoter from ZH11. The resultant vectors were transformed into rice calli of homozygous *nal1-cri* through Agrobacteria-mediated transformation. The positive transgenic lines were identified by PCR. Primers used in the PCR were shown in Extended Data Table 5.

To generate $NAL1^A$ introgression line, we crossed *indica* cultivar Huang-Hua-Zhan (HHZ) and *japonica* rice W118. Progenies containing the $NAL1^A$ allele (from W118) were backcrossed to HHZ for four generations and then self-crossed for three generations. Plants homozygous for $NAL1^A$ were selected from BC_4F_3 population and identified the phenotype in pot and field experiments.

Protein expression and purification

NAL1 was cloned into a modified *pET15D* vector and expressed in *E. coli* as 6×His-fusion. The construct was transformed into *E. coli* BL21 (DE3) and the cell cultures were grown at 37°C to OD600 of 1.0 - 1.2. Isopropyl-β-D-thiogalactoside of 0.2 mM was added to induce protein expression at 16°C for 12-16 h. The *E. coli* cells were harvested, homogenized in buffer A (25 mM Tris–HCl, pH 8.0, 150 mM NaCl), and lysed using a high-pressure cell disrupter (JNBIO, China). The cell lysates were centrifuged at 14,000 rpm for 1 h at 4°C. The supernatant containing soluble proteins was loaded onto a column equipped with Ni^{2+} affinity resin (Ni-NTA), washed with buffer B (25 mM Tris–HCl, pH 8.0, 150 mM NaCl, 15 mM imidazole), and eluted with buffer C (25 mM Tris–HCl, pH 8.0, 150 mM NaCl, 250 mM imidazole). The 6×His tag was removed by DrICE digestion. Then the digested protein was separated by cation exchange chromatography (Source 15Q, GE Healthcare) using buffer A with a linear NaCl gradient. The purified protein was concentrated and subjected to gel filtration chromatography (Superose 6, GE Healthcare) in a buffer containing 25 mM Tris-HCl, pH 8.0, 150 mM NaCl, 5 mM dithiothreitol. Proteins during all purification processes were subjected to SDS-PAGE and visualized by Coomassie blue staining. The peak

fractions were collected and stored at -80°C. NAL1 boundaries and mutants, as well as the seleno-methionine labeled proteins were purified similarly as the wild-type.

Crystallization, data collection, and structure determination

Protein was concentrated to 10 mg ml^{-1} before crystallization trials. Crystallizations were performed using the sitting-drop vapor diffusion method at 18°C by mixing an equal volume (1 μL) of protein with reservoir solution. Since our initial attempts to crystallize the full length NAL1 (residues 1–582) were unsuccessful, a series of truncations and cysteine mutations were performed. After several rounds of optimization, the crystal of a NAL1 construct (Q59-A463, C61S/C193S/C198S/C326S/C337S/C364S) appeared overnight and grew to full size within 3 days in the well buffer containing 0.1 M MES, pH 6.2, 0.1 M calcium acetate and 4% PEG6000. The crystals were flash-frozen in liquid nitrogen and cryoprotected by adding glycerol to a final concentration of 10%-20%.

The diffraction data were all collected at Shanghai Synchrotron Research Facility (SSRF) on beamline BL17U or BL19U. The data were integrated and processed with the HKL2000 program suite and XDS packages [62]. Further data processing was carried out using CCP4 suit [63]. The crystal structure of NAL1 was solved via single-wavelength anomalous diffraction (SAD) method at a resolution of 2.6 Å. The structure was iteratively built with COOT [64] and refined with PHENIX program [65]. Data collection and structure refinement statistic were summarized in Extended Data Table 1. All figures were generated using the program PyMOL (http://www.pymol.org/).

Analytical ultracentrifugation (AUC) analysis

The stoichiometry of NAL1 oligomer was investigated by AUC experiments, which were performed in a Beckman Coulter XL-I analytical ultracentrifuge using two-channel centrepieces. NAL1 was in solutions containing 25 mM Tris-HCl, pH 8.0, 150 mM NaCl. Data were collected by absorbance detection at 18°C for proteins at a concentration of approximately 0.6 mg mL^{-1} at a rotor speed of 35,000 rpm. The SV-AUC data were globally analyzed using the SEDFIT program and fitted to a continuous c(s) distribution model to determine the molecular mass.

IP-MS

Immunoprecipitation in combination with mass spectrometry (IP-MS) was performed to identify NAL1-interacting proteins. Total protein was extracted from the seedlings of NAL1-overexpression transgenic plants [7] and wild type ZH11. The extracted total protein was precipitated by anti-Flag magnetic agarose (A36797, Thermo Scientific) and washed 5 times with a PBS buffer (3 mM Na_2HPO_4, 155 mM NaCl, 1 mM KH_2PO_4, pH 7.4, 1×complete protease inhibitor cocktail). The beads were added to a loading buffer and boiled for 10 min, then were subjected to SDS-PAGE. After in-gel digestion, the samples were used for

mass spectrometry (Thermo Scientific, nano LC-Q EXACTIVE). Information about interacting proteins of NAL1 by IP-MS was shown in Extended Data Table 3.

BiFC and LCI assays

NAL1 and 10-AA deleted mutant *nal1-1* were respectively cloned into the C-terminal YFP fusion vector *pSPYCE(R)* and *OsTPR2* was cloned into N-terminal YFP fusion vector *pSPYNE(R)173*. The constructs were transformed into Agrobacteria GV3101. Different combinations as indicated were transiently expressed in tobacco leaves. After 48 h, the fluorescence was captured using a confocal microscope (LSM980, ZEISS).

NAL1 and 10-AA deleted mutant *nal1-1* were respectively cloned into the *pCAMBIA-1300-cLuc* and the full-length and truncations of *OsTPR2* were cloned into the *pCAMBIA-1300-nLuc* vectors. The constructs were transformed into Agrobacteria GV3101. Different combinations as indicated were transiently expressed in tobacco leaves. After 48 h, 1 mM luciferin was applied to the injected regions of the tobacco leaves. The Luc fluorescence signal was observed with CCD-imaging instrument (Tanon Science and Technology). Relative primer sequences are shown in Extended Data Table 5.

Co-immunoprecipitation

NAL1 and the 10-AA deleted mutant *nal1-1* were cloned into the GFP fusion vector *HGF*, and *OsTPR2* was cloned into the Flag fusion vector *pCAMBIA-1300-Flag*. Different combinations as indicated were transiently expressed in tobacco leaves. After 48 h, total protein from the infiltrated tobacco leaves was independently extracted in lysis buffer (50 mM Tris-HCl, pH 8.0, 150 mM NaCl, 0.5% Triton X-100, 1 mM EDTA, 1 mM PMSF and 1×complete protease inhibitor cocktail). Each protein extract was incubated with anti-Flag magnetic agarose (A36797, Thermo Scientific) for 4 h at 4°C, and washed 5 times with lysis buffer. The beads were added to loading buffer and boiled for 10 min, then samples were detected by western blot with anti-Flag and anti-GFP antibody.

Size exclusion chromatography

To further map the crucial residues that mediate the interactions between NAL1 and OsTPR2, a series of truncations or mutants were constructed and purified to homogeneity. Proteins as indicated were mixed, incubated for 1 h at room temperature, and further subjected to gel filtration chromatography (Superose 6, GE Healthcare) in a buffer containing 25 mM Tris, pH 8.0, 150 mM NaCl, 5 mM dithiothreitol. The relevant fractions of each independent injection were collected for SDS-PAGE analysis.

Cell-free protein degradation assays

The cell-free protein degradation assay was performed as described previously [23]. Total protein was extracted from the seedlings of ZH11 and *nal1-cri*, ZF802 and *nal1-1*, or NIL-IR and NIL-ZS with degradation buffer (25 mM Tris-HCl, pH 7.5, 10 mM NaCl, 10 mM $MgCl_2$, and 10 mM ATP). After two 10 min centrifugations at 12,000 rpm at 4°C, the supernatant was collected and the protein concentration was determined by A280 using NanoDrop 2000 Spectrophotometer (Thermo Scientific). Each cell-free degradation assay was performed in 250 μL degradation buffer including 500 μg total proteins, and 100 ng purified OsTPR2-N-His. For the different protease inhibitors treatment, total protein extracts from ZH11 were used and serine protease inhibitor (5 mM PMSF, 1 mM aprotinin or 1 mM leupeptin), metalloprotease inhibitor (0.5 mM bestain), aspartic protease inhibitor (1 μM pepstain) and cysteine protease inhibitor (10 μM E-64) was separately added into each mixture. The mixtures were incubated at 37°C. Equal volume of protein mixture was collected at indicated time (0, 10, 20, and 30 min) and subjected to western blot with anti-His antibody. Plant actin was used as the loading control.

In vivo protein degradation assays

30 μg OsTPR2-Flag or GFP plasmids were transfected into ZH11 and *nal1-cri*, ZF802 and *nal1-1*, or NIL-IR and NIL-ZS protoplasts. After 16 h incubation, protoplasts were treated with 200 μM protein synthesis inhibitor cycloheximide (CHX; Sigma-Aldrich) and gently mixed. Equivalent protoplasts were collected at indicated time (0, 1, 3, and 5 h). Total proteins were extracted with extraction buffer (50 mM Tris-HCl, pH 7.5, 150 mM NaCl, 10% glycerol, 0.1% IGEPAL CA-630, 1×complete protease inhibitor cocktail) and subjected to western blot with anti-Flag antibody (F3165, Sigma-Aldrich) and anti-GFP antibody (ab290, Abcam). GFP protein was used as a negative control.

In vitro protein degradation assays

The proteolytic activity of NAL1 to OsTPR2 was assayed in a reaction buffer (25 mM Tris-HCl, pH 7.5, 10 mM NaCl, and 10 mM $MgCl_2$, 10 mM ATP) including 0.2 mg purified His-tagged NAL1 or the triad-mutated NAL1 (mNAL1) and 0.2 mg purified StrepII-tagged OsTPR2 in a total volume of 200 μL. The mixtures were incubated at 37°C. Equal volume of protein mixture was collected at indicated time (0, 15, 30, and 60 min) and subjected to SDS/PAGE. Subsequently, the gels were stained with Coomassie Brilliant Blue R-250.

In vitro pull-down assays

OsARF25 and *IPA1* were separately cloned into GST-tagged *pGEX-6p-1* vector. OsIAA3/17 and D53 were separately cloned into His-tagged *pET32a* vector. OsTPR2 was cloned into StrepII-tagged *pMlink* vector. In the StrepII pulldown assays, purified recombinant proteins were added in StrepII-binding buffer (50 mM Tris-HCl, pH 8.0, 100 mM NaCl, 0.5% Triton X-100, 0.5% glycerol, 1 mM PMSF and 1×complete protease inhibitor cocktail) as indicated. Each protein mixture was incubated with StrepII beads (Sigma-Aldrich,

41246) for 4 h at 4°C and washed 5 times with binding buffer. After incubation, the beads were added to a 1×loading buffer and boiled for 10 min, and then samples were detected separately by western blot with anti-His and anti-GST antibody. The OsTPR2-StrepII was detected by Coomassie Brilliant Blue R-250.

ChIP-seq and ChIP-qPCR

3 g of ZH11 and *nal1-cri* seedlings were harvested and fixed for 30 min in 1% (v/v) formaldehyde under vacuum. Fixed tissues were homogenized, and chromatin was isolated and sonicated to produce DNA fragments around 300 base pairs. Then, anti-H3K18Ac (A7257, ABclonal) antibody with Dynabeads Protein A (10002D, Invitrogen) were added to the sonicated chromatin followed by incubation overnight at 4°C to precipitate antibody-bound DNA fragments. DNA was eluted and sequenced by Novogene Inc. (Beijing, China) with Illumina HiseqXten-PE150 and a paired-end sequencing strategy. The raw sequencing reads were filtered by fastp v0.23.1 (with the parameter "-q 30") [66] and mapped to rice genome assembly MSU v7.0 by bowtie2 v2.4.5 [67] with default parameters. Peak calling was performed on nonredundant, uniquely mapped reads by MACS2 v2.2.7.1 with parameters "-f BAMPE -q 0.05 –call-summits" [68]. Peaks called in at least two replicates were used for differential-modification analysis by R package DiffBind v3.6.1 [69] with its built-in DESeq2 analyzer. Peaks with |log2(fold change)| > 1 and FDR < 0.05 were defined as differentially modified regions and their associated genomic features were annotated by R package ChIPseeker [70]. For genomic track visualization, relative reads coverage of IP vs input was processed by bamCompare in deepTools v3.5.1 [71] with parameters "--scaleFactorsMethod SES -bs 1" and visualized in IGV [72].

For ChIP-qPCR, DNA fragments were sonicated to 500-1000 base pairs. After DNA was eluted, relative enrichment of each fragment was determined by qPCR. The ChIP DNA sample was quantified in triplicates. Primers used for the ChIP assays were listed in Extended Data Table 5.

RT-qPCR

Total RNA was extracted from seedlings of ZH11, *nal1-cri* and double mutant lines using *TransZol* (TransGen, Beijing, China). Reverse transcription was carried out with a cDNA synthesis kit (TransGen, Beijing, China). qPCR was performed using SYBR Green mix (Kuke, Wuhan, China) on an Applied Biosystems 7500 Fast Real-Time PCR System. Quantitative variations were calculated by the relative quantification method ($2^{-\Delta\Delta CT}$) and four independent repeated experiments were performed for each sample. Primers were shown in Extended Data Table 5.

Declarations

ACKNOWLEDGMENTS

We thank the staffs of the BL17U1/BL19U1 beamline of the National Center for Protein Sciences Shanghai (NCPSS) at the Shanghai Synchrotron Radiation Facility for assistance during data collection, and research associate Dr. Delin Zhang at the Center for Protein Research, Huazhong Agricultural University, for technical support.

This work was supported by Innovative Research Group Project of the National Natural Science Foundation of China (grant 31821005), the Key Program of National Natural Science Foundation of China (grant 31930080), the Foundation of Hubei Hongshan Laboratory (grant 2021hszd011, 2021hskf003), and the China Postdoctoral Science Foundation (grant 2019M652669). We thank the BaiChuan fellowship of College of Life Science and Technology, Huazhong Agricultural University, for funding support.

AUTHOR CONTRIBUTIONS

W.L., J.Y., P.Y., and L.X. designed the study; W.L., J.Y., Y.Z., F.Z., Y.Y., X.L., and H.W. performed all experiments. W.L., J.Y., Z.G., Y.C., and H.T. analyzed data. W.L., J.Y., H.X., X.L., and L.X. wrote and revised the article.

DECLARATION OF INTERESTS

The authors declare no competing interests.

References

1. Ray, D. K., Mueller, N. D., West, P. C. & Foley, J. A. Yield Trends Are Insufficient to Double Global Crop Production by 2050. PLoS One **8**, e66428 (2013).
2. Liu, M. *et al.* Inducible overexpression of *Ideal Plant Architecture1* improves both yield and disease resistance in rice. Nat Plants **5**, 389–400 (2019).
3. Xue, W. *et al.* Natural variation in Ghd7 is an important regulator of heading date and yield potential in rice. Nat Genet **40**, 761–767 (2008).
4. Weng, X. Y. *et al.* Grain Number, Plant Height, and Heading Date7 Is a Central Regulator of Growth, Development, and Stress Response. Plant Physiology **164**, 735–747 (2014).
5. Wang, Q. *et al.* The Ghd7 transcription factor represses ARE1 expression to enhance nitrogen utilization and grain yield in rice. Mol Plant **14**, 1012–1023 (2021).
6. Qian, Q., Guo, L. B., Smith, S. M. & Li, J. Y. Breeding high-yield superior quality hybrid super rice by rational design. Natl Sci Rev **3**, 283–294 (2016).
7. Li, X. *et al.* Genetic control of the root system in rice under normal and drought stress conditions by genome-wide association study. PLoS Genet **13**, e1006889 (2017).
8. Taguchi-Shiobara, F. *et al.* Natural Variation in the Flag Leaf Morphology of Rice Due to a Mutation of the NARROW LEAF 1 Gene in Oryza sativa L. Genetics **201**, 795–808 (2015).

9. Takai, T. *et al.* A natural variant of *NAL1*, selected in high-yield rice breeding programs, pleiotropically increases photosynthesis rate. Sci Rep **3**, 2149 (2013).
10. Wang, Q. *et al.* Genetic Architecture of Natural Variation in Rice Chlorophyll Content Revealed by a Genome-Wide Association Study. Mol Plant **8**, 946–957 (2015).
11. Yano, K. *et al.* Genome-wide association study using whole-genome sequencing rapidly identifies new genes influencing agronomic traits in rice. Nat Genet **48**, 927–934 (2016).
12. Zhang, G. H. *et al. LSCHL4* from *Japonica* Cultivar, which is allelic to *NAL1*, increases yield of *indica* super rice 93 – 11. *Mol Plant* **7**, 1350–1364 (2014).
13. Xu, J. L. *et al. SS1* (*NAL1*)- and *SS2*-Mediated Genetic Networks Underlying Source-Sink and Yield Traits in Rice (*Oryza sativa* L.). *PLoS One* **10**, e0132060 (2015).
14. Singh, V. K. *et al.* Effect of *qGN4.1* QTL for Grain Number per Panicle in Genetic Backgrounds of Twelve Different Mega Varieties of Rice. Rice (N Y) **11**, 8 (2018).
15. Fujita, D. *et al. NAL1* allele from a rice landrace greatly increases yield in modern *indica* cultivars. Proc Natl Acad Sci U S A **110**, 20431–20436 (2013).
16. Chen, M. *et al.* Fine mapping of a major QTL for flag leaf width in rice, *qFLW4*, which might be caused by alternative splicing of *NAL1*. Plant Cell Rep **31**, 863–872 (2012).
17. Ding, X., Li, X. & Xiong, L. Evaluation of near-isogenic lines for drought resistance QTL and fine mapping of a locus affecting flag leaf width, spikelet number, and root volume in rice. Theor Appl Genet **123**, 815–826 (2011).
18. Wang, Y. *et al.* Natural Sequence Variations and Combinations of *GNP1* and *NAL1* Determine the Grain Number per Panicle in Rice. Rice (N Y) **13**, 14 (2020).
19. Qi, J. *et al.* Mutation of the rice *Narrow leaf1* gene, which encodes a novel protein, affects vein patterning and polar auxin transport. Plant Physiol **147**, 1947–1959 (2008).
20. Lin, L., Zhao, Y., Liu, F., Chen, Q. & Qi, J. Narrow leaf 1 (NAL1) regulates leaf shape by affecting cell expansion in rice (*Oryza sativa* L.). Biochem Biophys Res Commun **516**, 957–962 (2019).
21. Cho, S.-H., Yoo, S.-C., Zhang, H., Lim, J.-H. & Paek, N.-C. Rice *NARROW LEAF1* Regulates Leaf and Adventitious Root Development. Plant Mol Biol Rep **32**, 270–281 (2013).
22. Jiang, D. *et al.* Characterization of a null allelic mutant of the rice *NAL1* gene reveals its role in regulating cell division. PLoS One **10**, e0118169 (2015).
23. Huang, Y. *et al.* Variation in the regulatory region of *FZP* causes increases in secondary inflorescence branching and grain yield in rice domestication. Plant J **96**, 716–733 (2018).
24. Ye, L. *et al.* A Trypsin Family Protein Gene Controls Tillering and Leaf Shape in Barley. Plant Physiol **181**, 701–713 (2019).
25. Plant, A. R., Larrieu, A. & Causier, B. Repressor for hire! The vital roles of TOPLESS-mediated transcriptional repression in plants. New Phytol **231**, 963–973 (2021).
26. Ryu, H., Cho, H., Bae, W. & Hwang, I. Control of early seedling development by BES1/TPL/HDA19-mediated epigenetic regulation of *ABI3*. Nat Commun **5**, 4138 (2014).

27. Wang, L., Kim, J. & Somers, D. E. Transcriptional corepressor TOPLESS complexes with pseudoresponse regulator proteins and histone deacetylases to regulate circadian transcription. Proc Natl Acad Sci U S A **110**, 761–766 (2013).
28. Long, J. A., Ohno, C., Smith, Z. R. & Meyerowitz, E. M. TOPLESS regulates apical embryonic fate in *Arabidopsis*. Science **312**, 1520–1523 (2006).
29. Tang, N. *et al.* MODD Mediates Deactivation and Degradation of OsbZIP46 to Negatively Regulate ABA Signaling and Drought Resistance in Rice. Plant Cell **28**, 2161–2177 (2016).
30. Deribe, Y. L., Pawson, T. & Dikic, I. Post-translational modifications in signal integration. Nat Struct Mol Biol **17**, 666–672 (2010).
31. Niu *et al.* SIZ1-Mediated SUMOylation of TPR1 Suppresses Plant Immunity in *Arabidopsis*. Mol Plant **12**, 215–228 (2019).
32. Causier, B., Ashworth, M., Guo, W. & Davies, B. The TOPLESS interactome: a framework for gene repression in *Arabidopsis*. Plant Physiol **158**, 423–438 (2012).
33. Gao, X. *et al. OsLIS-L1* encoding a lissencephaly type-1-like protein with WD40 repeats is required for plant height and male gametophyte formation in rice. Planta **235**, 713–727 (2012).
34. Jiang, L. *et al.* DWARF 53 acts as a repressor of strigolactone signalling in rice. Nature **504**, 401–405 (2013).
35. Fang, J. *et al.* The URL1-ROC5-TPL2 transcriptional repressor complex represses the *ACL1* gene to modulate leaf rolling in rice. Plant Physiol **185**, 1722–1744 (2021).
36. Zhuang, H. *et al. NONSTOP GLUMES1* Encodes a C2H2 Zinc Finger Protein That Regulates Spikelet Development in Rice. Plant Cell **32**, 392–413 (2020).
37. Hao, Y. *et al.* Genome-wide identification, phylogenetic analysis, expression profiling, and protein-protein interaction properties of *TOPLESS* gene family members in tomato. J Exp Bot **65**, 1013–1023 (2014).
38. Liu, X., Galli, M., Camehl, I. & Gallavotti, A. RAMOSA1 ENHANCER LOCUS2-Mediated Transcriptional Repression Regulates Vegetative and Reproductive Architecture. Plant Physiol **179**, 348–363 (2019).
39. Szemenyei, H., Hannon, M. & Long, J. A. TOPLESS mediates auxin-dependent transcriptional repression during *Arabidopsis* embryogenesis. Science **319**, 1384–1386 (2008).
40. Martin-Arevalillo, R. *et al.* Structure of the *Arabidopsis* TOPLESS corepressor provides insight into the evolution of transcriptional repression. Proc Natl Acad Sci U S A **114**, 8107–8112 (2017).
41. Ke, J. *et al.* Structural basis for recognition of diverse transcriptional repressors by the TOPLESS family of corepressors. Sci Adv **1**, e1500107 (2015).
42. Zhang, Z. *et al.* Gnp4/LAX2, a RAWUL protein, interferes with the OsIAA3–OsARF25 interaction to regulate grain length via the auxin signaling pathway in rice. J Exp Bot **69**, 4723–4737 (2018).
43. Gao, S. *et al. CYTOKININ OXIDASE/DEHYDROGENASE4* Integrates Cytokinin and Auxin Signaling to Control Rice Crown Root Formation. Plant Physiol **165**, 1035–1046 (2014).

44. Song, X. *et al.* IPA1 functions as a downstream transcription factor repressed by D53 in strigolactone signaling in rice. Cell Res **27**, 1128–1141 (2017).
45. Xu, X. *et al.* Pyramiding of the dep1-1 and NAL1(NJ6) alleles achieves sustainable improvements in nitrogen-use efficiency and grain yield in japonica rice breeding. J Genet Genomics **46**, 325–328 (2019).
46. Huang, X. *et al.* A map of rice genome variation reveals the origin of cultivated rice. Nature **490**, 497–501 (2012).
47. Wang, W. *et al.* Genomic variation in 3,010 diverse accessions of Asian cultivated rice. Nature **557**, 43–49 (2018).
48. Ouyang, M. *et al.* The crystal structure of Deg9 reveals a novel octameric-type HtrA protease. Nat Plants **3**, 973–982 (2017).
49. Tsiatsiani, Gevaert, Van & Breusegem. Natural substrates of plant proteases: how can protease degradomics extend our knowledge? Physiol Plant **145**, 28–40 (2012).
50. Ma, H. *et al.* A D53 repression motif induces oligomerization of TOPLESS corepressors and promotes assembly of a corepressor-nucleosome complex. Sci Adv **3**, e1601217 (2017).
51. Santner, A. & Estelle, M. Recent advances and emerging trends in plant hormone signalling. Nature **459**, 1071–1078 (2009).
52. Pauwels, L. *et al.* NINJA connects the co-repressor TOPLESS to jasmonate signalling. Nature **464**, 788–791 (2010).
53. Li, C. *et al. Arabidopsis* ECAP Is a New Adaptor Protein that Connects JAZ Repressors with the TPR2 Co-repressor to Suppress Jasmonate-Responsive Anthocyanin Accumulation. Mol Plant **13**, 246–265 (2020).
54. Wang, L. *et al.* Transcriptional regulation of strigolactone signalling in *Arabidopsis*. Nature **583**, 277–281 (2020).
55. Xu, M., Zhu, L., Shou, H. & Wu, P. A PIN1 Family Gene, OsPIN1, involved in Auxin-dependent Adventitious Root Emergence and Tillering in Rice. Plant Cell Physiol **46**, 1674–1681 (2005).
56. Duan, J. *et al.* Strigolactone promotes cytokinin degradation through transcriptional activation of *CYTOKININ OXIDASE/DEHYDROGENASE 9* in rice. Proc Natl Acad Sci U S A **116**, 14319–14324 (2019).
57. Laplaze, L. *et al.* Cytokinins Act Directly on Lateral Root Founder Cells to Inhibit Root Initiation. Plant Cell **19**, 3889–3900 (2007).
58. Zhao, Y. *et al.* The Interaction between Rice ERF3 and WOX11 Promotes Crown Root Development by Regulating Gene Expression Involved in Cytokinin Signaling. Plant Cell **27**, 2469–2483 (2015).
59. Ouyang, X. *et al.* Partially functional NARROW LEAF1 balances leaf photosynthesis and plant architecture for greater rice yield. Plant Physiol **189**, 772–789 (2022).
60. Zhang, Q. *et al.* Genomic insights into the recent chromosome reduction of autopolyploid sugarcane Saccharum spontaneum. Nat Genet **54**, 885–896 (2022).

61. He, Y. *et al.* Programmed Self-Elimination of the CRISPR/Cas9 Construct Greatly Accelerates the Isolation of Edited and Transgene-Free Rice Plants. Mol Plant **11**, 1210–1213 (2018).
62. Otwinowski, Z. & Minor, W. Processing of X-ray Diffraction Data Collected in Oscillation Mode. Methods Enzymol **276**, 307–326 (1997).
63. Winn, M. D. *et al.* Overview of the CCP4 suite and current developments. Acta Crystallogr D Biol Crystallogr **67**, 235–242 (2011).
64. Emsley, P. & Cowtan, K. Coot: model-building tools for molecular graphics. Acta Crystallogr D **60**, 2126–2132 (2004).
65. Adams, P. D. *et al.* PHENIX: building new software for automated crystallographic structure determination. Acta Crystallogr D Biol Crystallogr **58**, 1948–1954 (2002).
66. Chen, S., Zhou, Y., Chen, Y. & Gu, J. *fastp*: an ultra-fast all-in-one FASTQ preprocessor. *Bioinformatics* **34**, i884-i890 (2018).
67. Langmead, B. & Salzberg, S. L. Fast gapped-read alignment with Bowtie 2. Nat Methods **9**, 357–359 (2012).
68. Zhang, Y. *et al.* Model-based analysis of ChIP-Seq (MACS). Genome Biol **9**, R137 (2008).
69. Ross-Innes, C. S. *et al.* Differential oestrogen receptor binding is associated with clinical outcome in breast cancer. Nature **481**, 389–393 (2012).
70. Yu, G., Wang, L. G. & He, Q. Y. ChIPseeker: an R/Bioconductor package for ChIP peak annotation, comparison and visualization. Bioinformatics **31**, 2382–2383 (2015).
71. Ramirez, F., Dundar, F., Diehl, S., Gruning, B. A. & Manke, T. deepTools: a flexible platform for exploring deep-sequencing data. Nucleic Acids Res **42**, W187-W191 (2014).
72. Robinson, J. T. *et al.* Integrative genomics viewer. Nat Biotechnol **29**, 24–26 (2011).

Figures

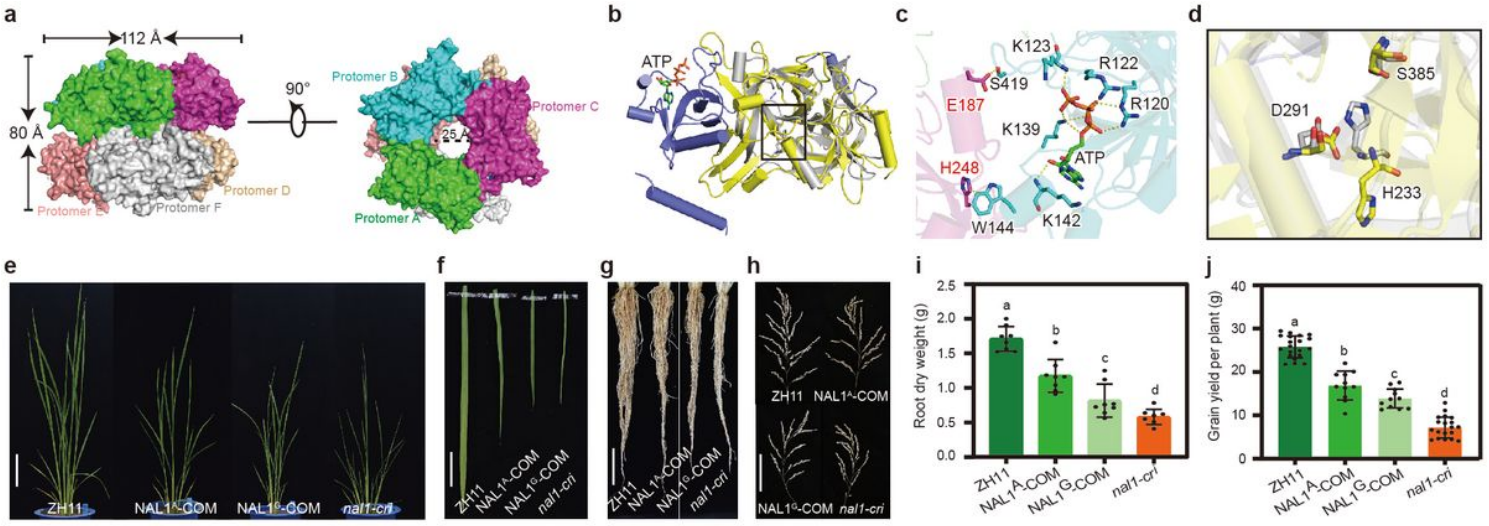

Figure 1

Crystal structure of NAL1 hexamer. **a**, Overall structure of NAL1. The side and top view of NAL1 hexamer. The trimeric rings in the right panel reveals the arrangement of the NTD and protease domain involved in the oligomeric assembly. **b**, Structural superposition between NAL1 and a serine protease. Slate and yellow indicate NTD and protease domain of NAL1, respectively. ATP molecule in the NTD is indicated in sticks. The serine protease is colored in gray (PDB ID: 1P01). **c**, ATP molecule-mediated protomer interaction network. ATP is embedded in a positively charged pocket. Sticks indicate key residues. **d**, Putative catalytic triad of NAL1. Yellow sticks denote the residues. **e–h**, Plant architecture and yield-related traits of wild type (ZH11), two complementary lines (*NAL1*^{A}-COM and *NAL1*^{G}-COM), and *NAL1*-knockout line (*nal1-cri*). (**e**) Plant morphology, bar = 20 cm. (**f**) Flag leaf morphology, bar = 5 cm. (**g**) Root system, bar = 5 cm. (**h**) Panicle structure, bar = 2 cm. **i** and **j**, Comparisons among ZH11, two complementary lines, and *nal1-cri*. (**i**) Root dry weight (n = 8). (**j**) Grain yield per plant (n >=10). Different lowercase letters above bars indicate significant difference at $P < 0.05$ level.

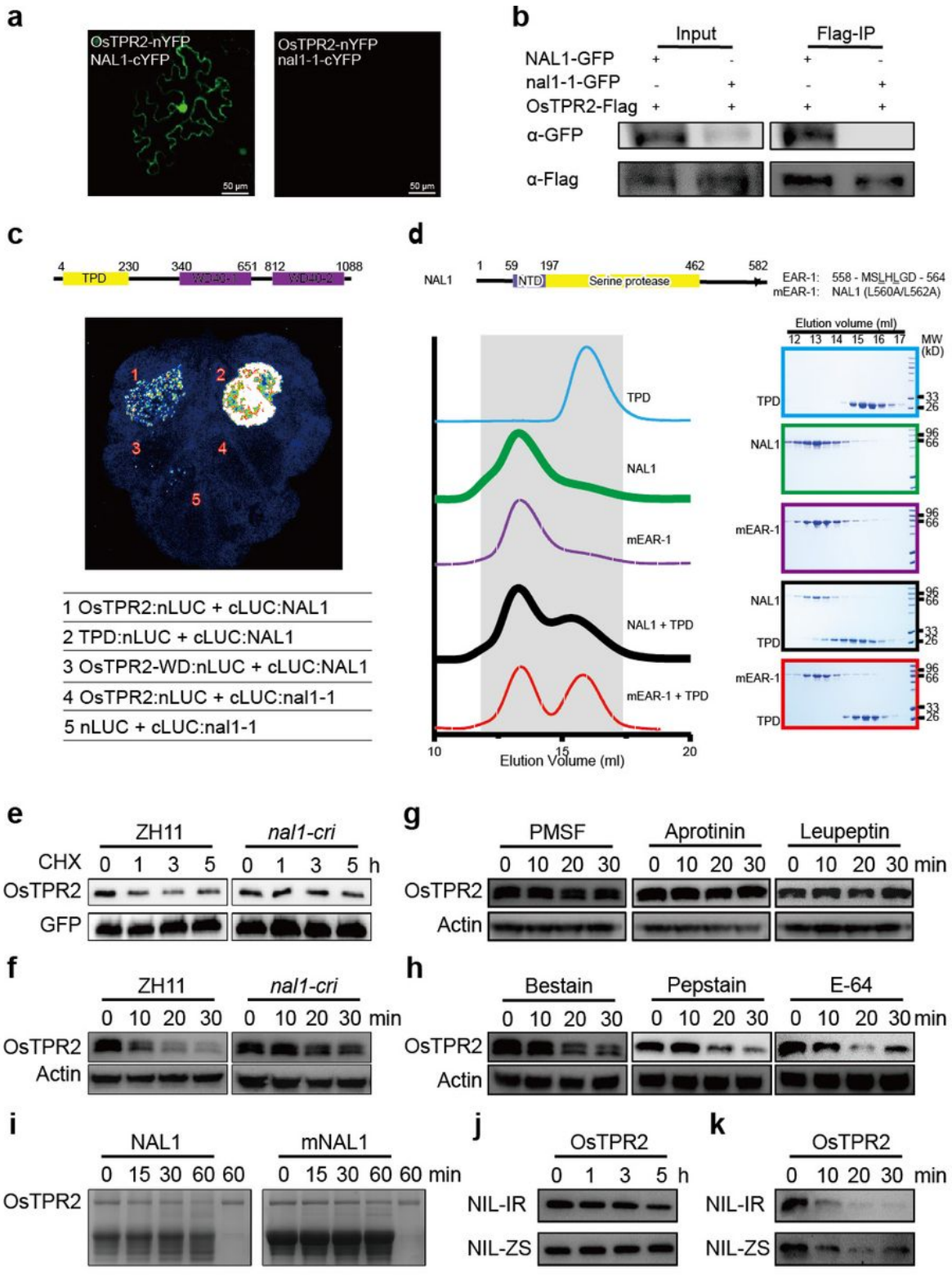

Figure 2

NAL1 targets OsTPR2 for degradation. a, Interaction between NAL1 and OsTPR2 in tobacco leaves by BiFC assays. Bar = 50 μm. **b**, Interaction between NAL1 and OsTPR2 in tobacco leaves by a co-immunoprecipitation assay. **c**, Interaction between NAL1 and N-terminal of OsTPR2 (TPD) in tobacco leaves by LCI assays. The 10-AA deletion mutant nal1-1 was used as a negative control. **d**, Interactions between NAL1 and OsTPR2 by size-exclusion chromatography analysis. Fractions with the same elution

volume from each injection were subjected to SDS-PAGE. **e**, Degradation of OsTPR2 in ZH11 and *nal1-cri* protoplasts after cycloheximide (CHX) treatment. Transfected rice protoplasts were incubated for 16 h, and then treated with (50 g ml^{-1}) CHX to block protein synthesis. Equal volume of protoplasts were collected at different time points for immunoblotting detection of OsTPR2. GFP was used as a loading control. **f**, Degradation of total protein extract from ZH11 and *nal1-cri* seedlings by cell-free protein degradation assays. 6×His-tagged OsTPR2 was respectively added to total protein extract from ZH11 and *nal1-cri* plants. Equal volume of protein mixture was collected at different time points for immunoblotting detection of OsTPR2. **g**, NAL1 proteolytic activity was inhibited by serine protease inhibitor in cell-free protein degradation assays. Degradation of OsTPR2 by total protein extract from ZH11 seedlings after adding different serine protease inhibitors (5 mM PMSF, 1 mM aprotinin or 1 mM leupeptin). **h**, NAL1 proteolytic activity was not inhibited by other protease inhibitors in cell-free protein degradation assays. Degradation of OsTPR2 by total proteins extract from ZH11 seedlings after adding metalloprotease inhibitor (0.5 mM bestain), aspartic protease inhibitor (1 μM pepstain), or cysteine protease inhibitor (10 μM E-64). Actin was as a loading control. **i**, Degradation of OsTPR2 *in vitro*. NAL1 or the triad-mutated NAL1 (mNAL1) proteins were incubated with OsTPR2 for 15, 30, or 60 min at 37°C. A mixture without NAL1 or mNAL1 was used as a negative control. After terminating the reaction, the reaction mixtures were subjected to SDS/PAGE. Locations of OsTPR2 was indicated in the gel. **j**, Degradation of OsTPR2 in NIL-IR ($NAL1^{A}$) and NIL-ZS ($NAL1^{G}$) protoplasts after CHX treatment. Transfected rice protoplasts were incubated for 16 h, and then treated with (50 g ml-1) CHX to block protein synthesis. Equal volume of protoplasts were collected at different time points for immunoblotting detection of OsTPR2. **k**, Degradation of OsTPR2 in total protein extract from NIL-IR and NIL-ZS seedlings by cell-free protein degradation assays. 6×His-tagged OsTPR2 was respectively added to total protein extracts from NIL-IR and NIL-ZS plants. Equal volume of protein mixture was collected at different time points for immunoblotting detection of OsTPR2.

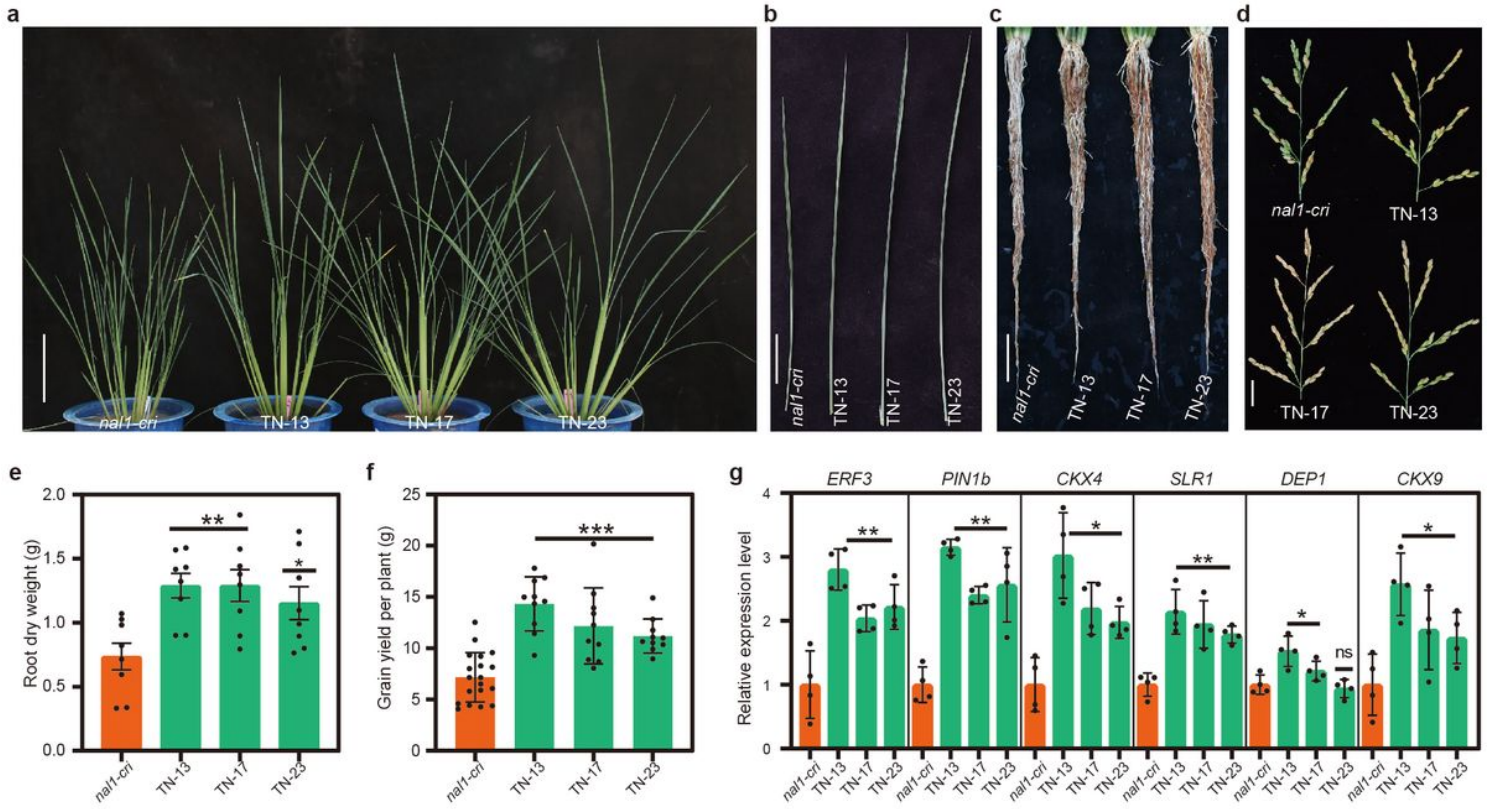

Figure 3

***OsTPR2* functions genetically downstream of *NAL1*. a-d**, Phenotypes of *nal1-cri* mutant and *OsTPR2*-knockdown lines in the *nal1-cri* background (named TN lines). (**a**) Plant morphology, bar = 20 cm. (**b**) Flag leaf morphology, bar = 5 cm. (**c**) Root system, bar = 5 cm. (**d**) Panicle structure, bar = 2 cm. **e-f**, Comparisons between *nal1-cri* and the TN lines. (**e**) Root dry weight, n = 8. (**f**) Grain yield per plant (n >10). *, **, and *** indicate significant differences at $P < 0.05$, 0.01, and 0.001 levels. **g,** Relative expression levels of auxin and SL signaling pathway genes in the seedlings of *nal1-cri* and TN lines. RT-qPCR was repeated for four times (n = 4). * and ** indicate significant differences at $P < 0.05$ and 0.01 levels. ns indicates no significant difference.

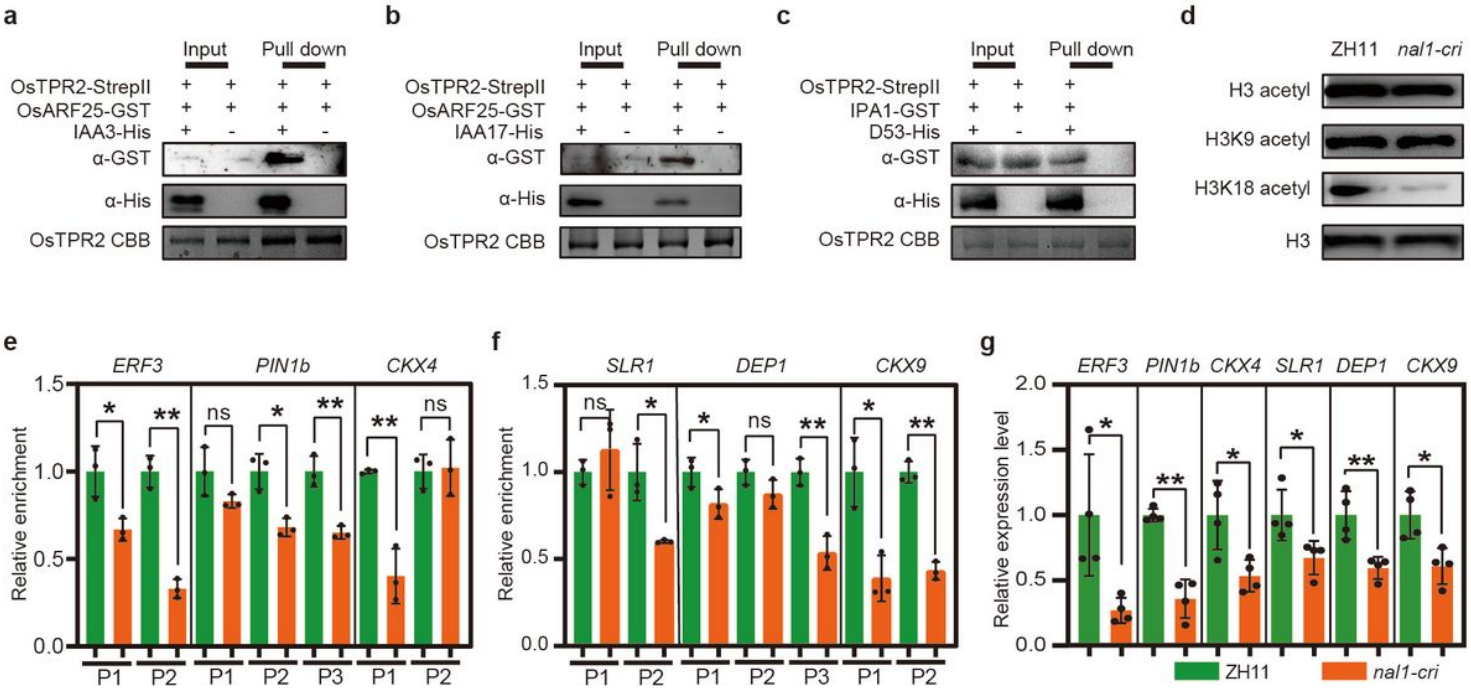

Figure 4

***NAL1* affects expression of auxin and SL signaling pathway genes. a-c,** Interactions were examined using pull-down assays. (**a**) Interaction among OsTPR2, OsARF25 and IAA3. (**b**) Interaction among OsTPR2, OsARF25 and IAA17. (**c**) Interaction among OsTPR2, IPA1, and D53. StrepII-tagged OsTPR2, GST-tagged OsARF25/IPA1, and 6×His-tagged IAA3/IAA17/D53 were incubated as indicated in (**a**-**c**) and then loaded onto StrepII beads for pull-down assays. OsARF25/IPA1 and IAA3/IAA17/D53 proteins were detected by immunoblot with anti-GST and anti-His antibodies. OsTPR2 protein was subjected to SDS/PAGE and detected by CBB. **d**, Histone acetylation levels in ZH11 and *nal1-cri*. H3 acetylation levels of total histone extract from ZH11 and *nal1-cri* seedlings were detected by immunoblot with anti-H3Ac, anti-H3K9Ac, and anti-H3K18Ac antibodies, respectively. H3 was used as a loading control. **e-f,** H3K18 acetylation levels of auxin (**e**) and SL (**f**) signaling pathway genes in ZH11 and *nal1-cri* by ChIP-qPCR. Data were fold changes relative to levels of ZH11 seedlings (n = 3). * and ** indicate significant differences at 0.05 and 0.01 levels. ns indicates no significant difference. **g,** Relative expression levels of auxin and SL signaling pathway genes in ZH11 and *nal1-cri* by RT-qPCR (n = 4). * and ** indicate significant differences at $P <$ 0.05 and 0.01 levels.

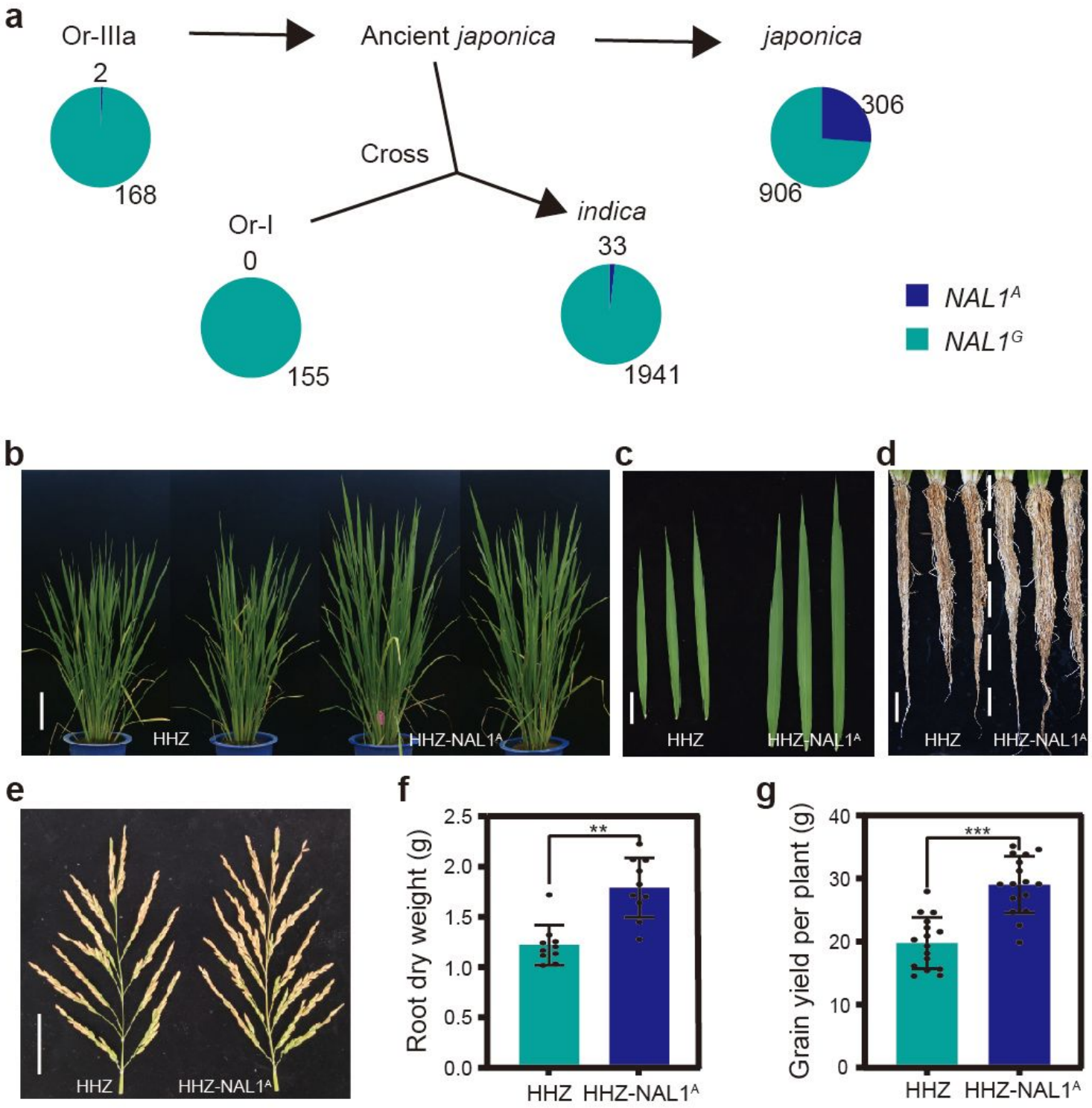

Figure 5

Functionally strong allele *NAL1*^{A} originated from common wild rice improves grain yield. a, Schematics of the origin of functionally strong allele *NAL1*^{A}. The frequency of two alleles (*NAL1*^{A} and *NAL1*^{G}) in 325 *O. rufipogon* accessions, 1974 *indica* varieties, and 1212 *japonica* varieties was estimated. **b-e,** Yield-related traits of Huang-hua-zhan (HHZ) and the *NAL1*^{A} introgression line (HHZ-NAL1^A). (**b**) Plant morphology, bar = 20 cm. (**c**) Flag leaf, bar = 5 cm. (**d**) Root system, bar = 5 cm. (**e**) Panicle structure, bar = 2 cm. **f-g,**

Comparisons between HHZ and HHZ-NAL1^{A}. (**f**) Root dry weight (n = 8). (**g**) Grain yield per plant (n >20). ** and *** indicate significant differences at $P < 0.01$, and 0.001 levels.

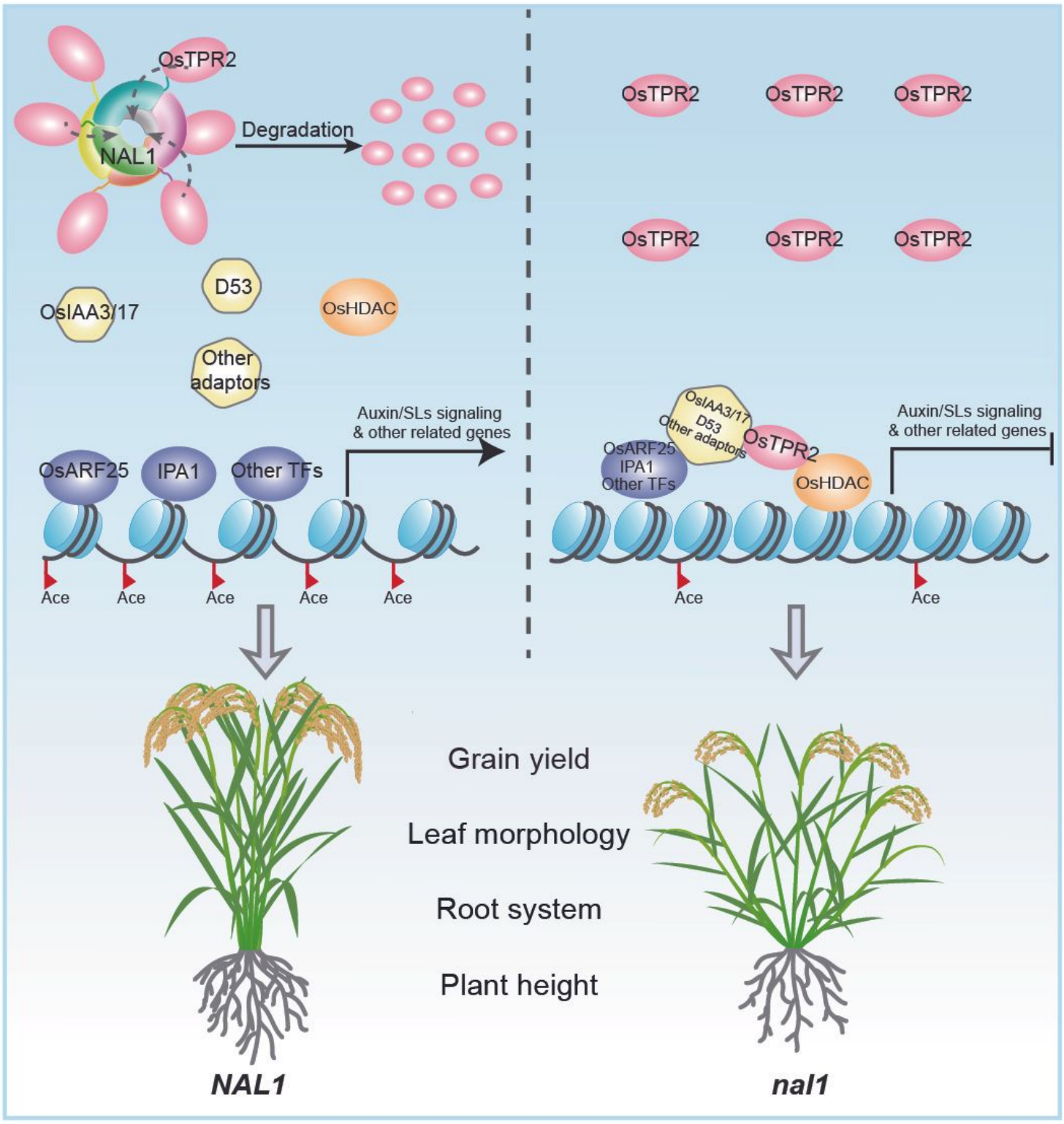

Figure 6

A proposed working model for the NAL1 pleiotropic function through OsTPR2 degradation. NAL1 forms a novel hexameric structure and interacts with the TOPLESS-related corepressor OsTPR2 via a C-terminal

EAR-like motif. In wild type (*NAL1*), NAL1 promotes the degradation of OsTPR2, resulting in the normal expression levels of downstream genes, finally maintaining a normal growth and development. However, the mutant *nal1* lacks the protease activity, thus leading to the enrichment of OsTPR2 protein and significant decrease in expression levels of downstream genes, eventually inducing pleiotropic traits such as less grain yield, narrower flag leaf, lower plant height, smaller root and panicle size.

Supplementary Files

This is a list of supplementary files associated with this preprint. Click to download.

- ExtendeddataTable1.xlsx
- ExtendeddataTable2.xlsx
- ExtendeddataTable3.xlsx
- ExtendeddataTable4.xlsx
- ExtendeddataTable5.xlsx
- ExtendeddataFig.1.jpg
- ExtendeddataFig.2.jpg
- ExtendeddataFig.3.jpg
- ExtendeddataFig.4.jpg
- ExtendeddataFig.5.jpg
- ExtendeddataFig.6.jpg
- ExtendeddataFig.7.jpg
- ExtendeddataFig.8.jpg
- ExtendeddataFig.9.jpg
- ExtendedDataFigureLegends.docx